Mathematical Biosciences and Engineering

MBE, 21(4): 5181–5206.
DOI: 10.3934/mbe.2024229
Received: 09 January 2024
Revised: 26 February 2024
Accepted: 27 February 2024
Published: 06 March 2024

http://www.aimspress.com/journal/MBE

*Research article*

# Study on synergistic effect of multiple physical fields on hot mix asphalt during compaction process

**Huanan Yu[1,*], Yutang Gao[1], Guoping Qian[1,2], Chao Zhang[1], Changyun Shi[1], Jinguo Ge[1] and Wan Dai[1]**

[1] National Engineering Research Center of Highway Maintenance Technology, School of Traffic and Transportation Engineering, Changsha University of Science & Technology, Changsha 410114, China
[2] Xiangjiang Laboratory, Changsha 410205, China

* **Correspondence:** Email: Huanan.yu@csust.edu.cn.

**Abstract:** The multiple physical fields of hot mix asphalt (HMA) during the compaction process have a significant impact on the durability of asphalt pavement, and this research aimed to evaluate the synergistic effect of the HMA field compaction of multi-physical field evolution during the compaction process. First, the temperature field, structural layer thickness variation, and structural layer density variation were monitored during field compaction. Second, the evolution properties of compaction thickness were obtained under the synergistic influence of multi-physical fields by temperature field and compaction thickness. Finally, the evolution properties of compaction density were obtained under the synergistic influence of multi-physical fields based on the temperature field and structural layer density. The results showed that the field compaction process could be characterized by three stages under the synergistic impact of multi-physical fields. The cooling of the temperature field presents two-stage characteristics. There were cubic polynomial evolution properties for the temperature field versus time and the density versus temperature field. There was an exponential relationship between the thickness of the compacted layer and the number of mills. The aggregate particles showed different motion characteristics in the horizontal and vertical directions and vertical directions. The vertical displacement was larger than the horizontal displacement under the synergistic influence of multi-physical fields during the three stages of compaction. The migration and reorganization of aggregate particles affected the evolution of the multi-physics fields of the compaction process under the action of different compaction modes.

**Keywords:** hot mix asphalt (HMA); field compaction process; temperature field; multiple physical

field; aggregate particle movement

## 1. Introduction

### *1.1. Research background*

Construction compaction is a critical component in enhancing the durability of asphalt pavement, and construction control is a cost-effective means. Therefore, many scholars have done macroscopic and microscopic simulations, digital graphic processing analyses, and indoor comparative tests on HMA (hot mix asphalt) to simulate the compaction process under the influence of multi-physical fields to improve the compaction quality.

Some scholars have devoted themselves to simulating the compaction process of HMA in the laboratory environment to reduce the void ratio of HMA field compaction in the past decades. Relevant studies have shown that pavement fatigue life could be increased by 10% with a 1% reduction in the void ratio of the mixture during compaction [1]. Zhao et al. found that the superpave gyratory compactor (SGC) and the shear box compactor (SBC) could better reproduce the field compaction condition by comparing the specimens compacted and shaped by the Marshall compactor, SSRC, SGC, SBC, and roller, among these methods [2].

Several methods using computers to simulate the compaction process of HMA have emerged with the rapid development of computer processing technology, for example, the analytical method, finite element method (FEM) [3], and discrete element method (DEM) [4]. Some scholars have used FEM to simulate the mechanical response of asphalt mixtures under different compaction methods [5]. Some scholars have used DEM first to simulate the motion properties of aggregate in the Marshall compaction test and then used the time-temperature equivalence principle to simulate the motion properties of aggregate under the changing temperature field during the compaction process [6,7]. However, most DEM research was the modeling of aggregates as spheres or spheroidal conglomerates [8], which did not produce accurate virtual aggregates or aggregate stacks, and the temperature of the compaction process in the field did not ideally vary linearly. It has been shown that the compaction of mixes varies with the temperature [9–11]. Significant reductions in voids in total mix (VTM) and voids in mineral aggregates (VMA) were obtained when the HMA compaction temperature was increased from 70 to 100 °C [12,13]. However, when the compaction temperature was lower than 85 °C, the VTM increased significantly [14].

To more comprehensively represent the influence of macro and micro features and aggregate morphology during HMA compaction, Liu et al. developed a coupled FEM-DEM model to maximize the balance between macro and micro elements [15]. However, the accuracy of their results needed to be further investigated. Komaragiri et al. optimized the morphological characteristics of aggregates by simulation using a physics engine [16,17], but the effects of factors have yet to be considered, such as friction between aggregates and the viscosity of the mortar in the physics engine. Although these techniques simulated the motion of aggregate particles to a certain extent, their accuracy still required further research under the synergistic influence of multiple physical fields.

SmartRock was widely used to further validate the accuracy of DEM for compaction simulation. SmartRock could track the motion of aggregate particles during compaction [18,19]. It has been found that the compaction process was not only related to the contact force between the aggregates [20,21],

but also to the size of the aggregate particles [22,23] and the vibration acceleration of the roller [24,25]. It has also been found that changes in compaction height could be translated into changes in the relative rotation of aggregate particles [26]. It has been found that gyratory compaction could better simulate the rolling process of rubber wheel rollers [27], and the locking point of the mixture was obtained by gyratory compaction [28]. However, the diameter of the SmartRock was too large (nearly 25 mm), which not only affected the gradation of the HMA but also generated stress concentrations around it, which affected the accuracy of the data.

In recent years, digital graphic processing techniques have been gradually applied to HMA compaction research. The migration and rotation properties of aggregates in the compaction process of the mixture were found through the statistical analysis of digital graphs [29]. It introduced some indicators, such as aggregate contact point and inclination angle, to characterize the skeleton properties of the mix [30,31]. It has been found that the shape-shadow characteristics of aggregates affected the mechanical properties of mixtures [32,33]. Image analysis of void distribution found that gyratory compaction was the closest to field compaction results [34]. These methods have achieved some aggregate motion characteristics and skeleton structure results. However, it was still unable to accurately describe the compaction properties of HMA under the influence of multiple physical fields.

The compaction of HMA could be improved by controlling compaction and changing the compaction method. Some scholars used DEM to model the interaction between asphalt mixture, and some used screed [35] to improve the compaction quality of HMA by controlling pre-compaction quality. Other scholars have also found that vacuum compaction could effectively improve the compaction of asphalt mixtures by comparing vacuum compaction with ordinary compaction [36] and compaction in different vacuum states [37].

A review of the literature reveals that there have been several studies on the effect of temperature field during HMA compaction as well as the kinematic properties of aggregate particles [38]. However, the former was more often studied by considering a single factor and using experimental and computer simulation methods. Studies assessing multiple physical fields still need to be included in the field on the HMA compaction process under field compaction conditions, and more effective and concise modeling studies still need to be included under the synergistic influence of multiple physical fields.

### *1.2. Objective and scope*

This research aimed to discover the synergistic influence between multi-physical fields by examining the evolution patterns of physical fields, such as temperature, thickness, and density, in the field compaction process, as well as to research the motion properties of aggregate particles in horizontal and vertical directions under the synergistic influence of multi-physical fields and the effect of aggregate migration and reorganization on the multi-physical fields. The research plans are shown in Figure 1.

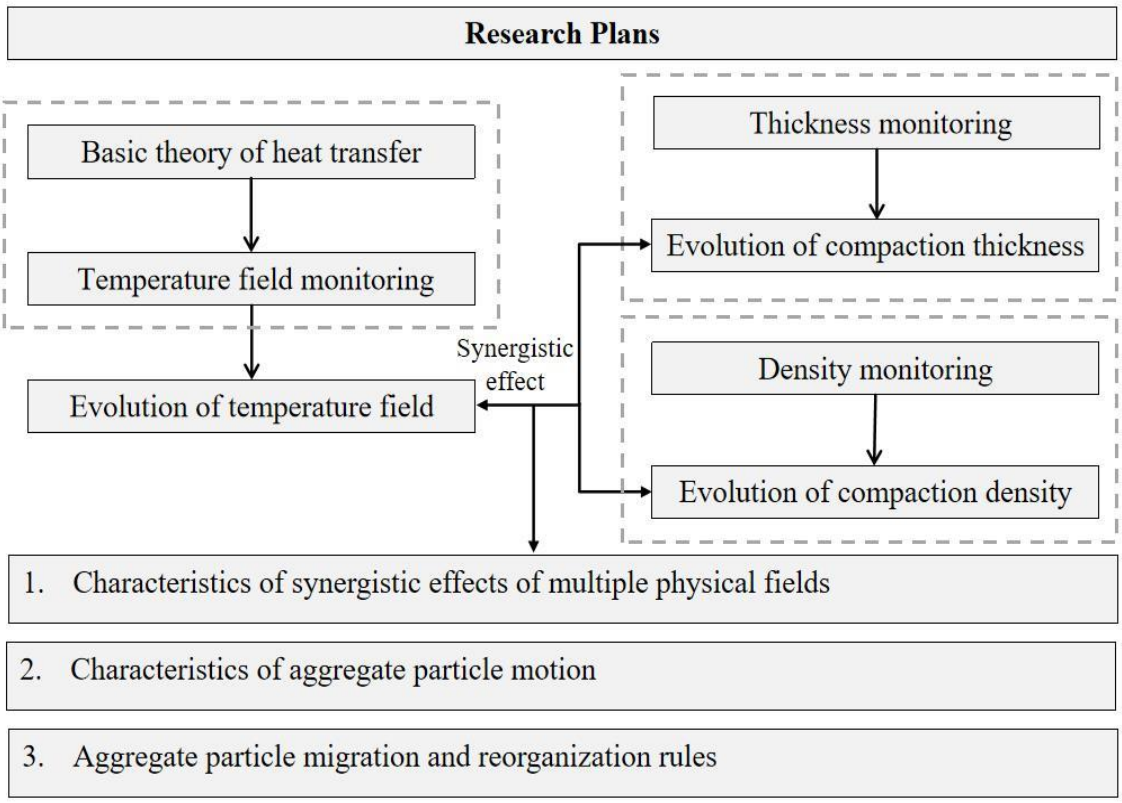


**Figure 1.** Research flowchart.

## 2. Theory of heat transfer

### *2.1. Basic heat transfer method*

The heat transfer process of HMA field compaction mainly consists of three basic heat transfer modes: heat conduction, heat convection, and heat radiation.

The heat transfer process of HMA field compaction is represented in Figure 2, and the process of heat transfer conforms to Fourier's law of heat transfer [39] as shown in Eq (1):

$$q(r,t) = -\lambda gradT(r,t) = -\lambda \nabla T(r,t) \tag{1}$$

where q is heat flux density, r is the proportionality factor, λ is thermal conductivity, and T (r, t) is temperature function.

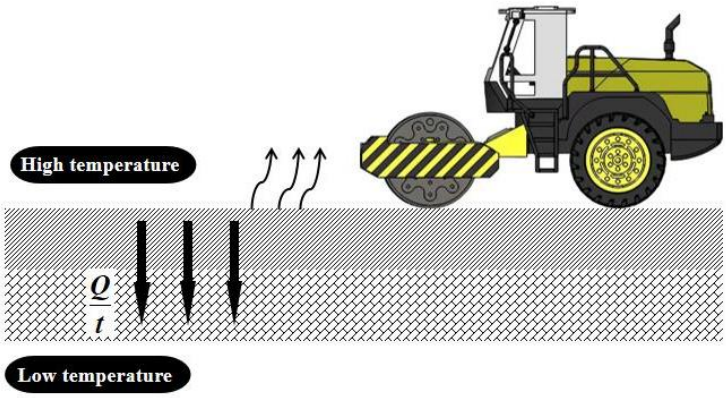


**Figure 2.** Heat transfer during compaction process.

In Figure 2, $t$ is the time, and $Q$ is the amount of heat transfer during time $t$.

The HMA compaction process satisfied the heat transfer equation [40], as in Eq (2):

$$\frac{\partial^2 T}{\partial^2 x}+\frac{\partial^2 T}{\partial^2 y}+\frac{\partial^2 T}{\partial^2 z}+\frac{q}{k}=\frac{1}{\alpha}\times\frac{\partial T}{\partial t} \tag{2}$$

where $\alpha$ is the thermal diffusion coefficient, $\alpha=\dfrac{k}{\rho c_p}$ indicates the ability of the internal temperature of an object to converge to a uniform temperature during unsteady-state heat transfer, $\rho$ is the density, $c_p$ is the constant-pressure specific heat capacity, $k$ is the thermal conductivity, and $q$ is the heat flow density.

Thermal convection phenomenon was generated on the contact surface between the mix and the air during HMA field compaction, and the total heat transfer coefficient between the air and the mix surface could be calculated by Newton's law of cooling [41], as in Eq (3):

$$\mathrm{q}=h\Delta t \tag{3}$$

where $h$ is the convective heat transfer coefficient of the substance and $\Delta t=\left|t_w-t_f\right|$ is the temperature difference between the object and the surrounding environment.

Thermal radiation is generated by the energy emitted from the material's surface. HMA could be regarded as a blackbody, so it satisfies the Stefan-Boltzmann [39] law as in Eq (4):

$$j^*=\varepsilon\sigma T_s^4 \tag{4}$$

where $j^*$ is the total power radiated per unit area of a blackbody surface, $\varepsilon$ is the radiation coefficient of the blackbody $0<\varepsilon<1$, $\sigma$ is the Stefan-Boltzmann constant, and $T_s$ is the thermodynamic temperature of the blackbody surface.

### *2.2. Transient nonlinear heat transfer*

There was a nonlinear behavior of the thermal properties of HMA during paving and compaction as a function of temperature, density, and boundary conditions. The heat balance equation for nonlinear thermal analysis is shown in Eq (5) [39]:

$$[C(T)]\{\dot{T}\}+[K(T)]\{T\}=\{Q(T)\} \tag{5}$$

The thermal properties of a material are a function of temperature. For example, the boundary conditions of K(T) and C(T) vary continuously with temperature simultaneously. The environment's temperature during the paving and rolling process played an essential role in the heat dissipation of HMA.

In summary, the variation of the temperature field of HMA was not only affected by boundary conditions, such as the initial temperature of the material and the external environment, but also by the density of the material during compaction. The mix's temperature, thickness, and density constantly changed during the compaction process, affecting the heat transfer rate of HMA. It showed a synergetic influence between the temperature field, compaction thickness ("compacted thickness" means the thickness of the field-compacted layer of HMA mixture.), and density.

## 3. Experiments

The temperature field was continuously monitored at the layer surface, middle, and bottom during the field compaction process to research the synergistic effect of multi-physical fields of HMA field compaction. The compaction thickness and density were continuously measured under different compaction methods with the constantly changing temperature field.

### *3.1. Project conditions*

Two representative projects were selected with the Jinpen Avenue project in the South China hot and humid weather and the Yuzhou-Dengfeng Expressway project in the North China dry weather.

### *3.2. Temperature field monitoring*

The temperature field monitoring relied on the asphalt pavement construction project of Jinpen Avenue in Changsha. The structure of the applied surface layer was designed as 3 cm AC-10 + 4 cm AC-16 + 8 cm AC-25 base asphalt concrete, and the measurement layer was 4 cm AC-16 asphalt concrete. At that time, the temperature was 15°C, the wind speed was 3~4 grade, and it was cloudy. The double drum rollers all used the steel wheel static pressure mode, and the design rolling process was four times (eight times for the same section).

Pt100 temperature sensors should be buried within the asphalt mixture layer immediately after paving to test the consistency of HMA heat transfer at different locations. The final locations were doubled checked and it was found that all sensors were within 2 mm error of the design location, which satisfied the design requirement. Two measurement points were randomly selected on the road section as P1 and P2, and sensors B1, B2, and B3 were buried in the paving layer's surface, middle, and bottom,

as shown in Figure 3 below. The data collection was started before the initial compaction by the roller to measure the temperature change of the layer surface, middle of the layer, and the bottom bearing layer surface in the compaction process.

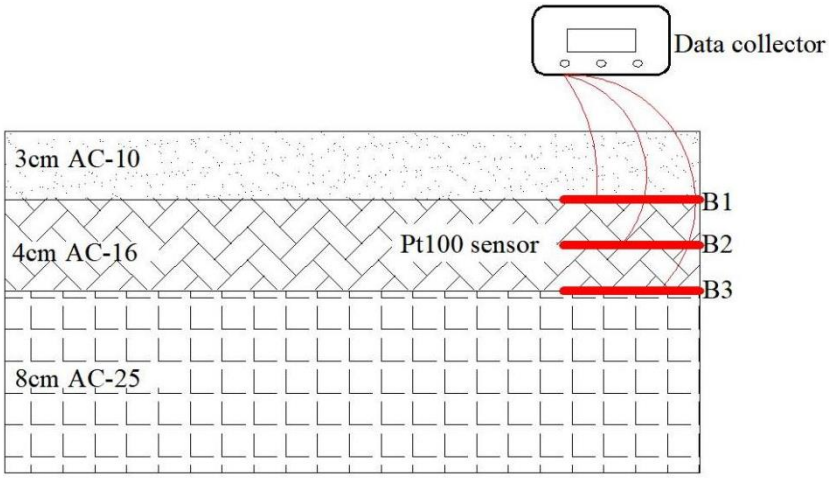


**Figure 3.** Temperature sensor burial location.

### *3.3. Thickness monitoring*

The monitoring work of thickness change also relied on the construction project of the middle surface layer AC-16 in the compaction process of HMA. Four measurement sections were selected, namely, M1, M2, M3, and M4, and two measurement points were randomly selected for each measurement section, namely, A1 and A2. Elevation measurements were carried out every time the steel-wheel roller rolled once (i.e., including two round trips). The evolution properties of the compaction thickness and the movement properties of the aggregate particles in the horizontal and vertical directions were obtained under the synergistic influence of multi-physical fields by measuring the compaction thickness.

### *3.4. Density monitoring*

The compaction density monitoring was based on the construction project of the upper layer of asphalt pavement of the Yuzhou-Dengfeng Expressway. The design structure of the construction surface layer was 5 cm AC-16C + 6 cm AC-20C + 8 cm AC-25C of modified asphalt concrete, as shown in Figure 4. The design process of construction rolling was: The initial pressure was one time the static pressure of 13 t double drum roller, the design of repressing was seven times the vibration pressure of 13 t double drum roller and 6 times the 26 t tire roller, and the final pressure was four times the 11 t dual static pressure. Design speed: steel wheel traveling speed of 4 km/h and rubber wheel traveling speed of 6 km/h.

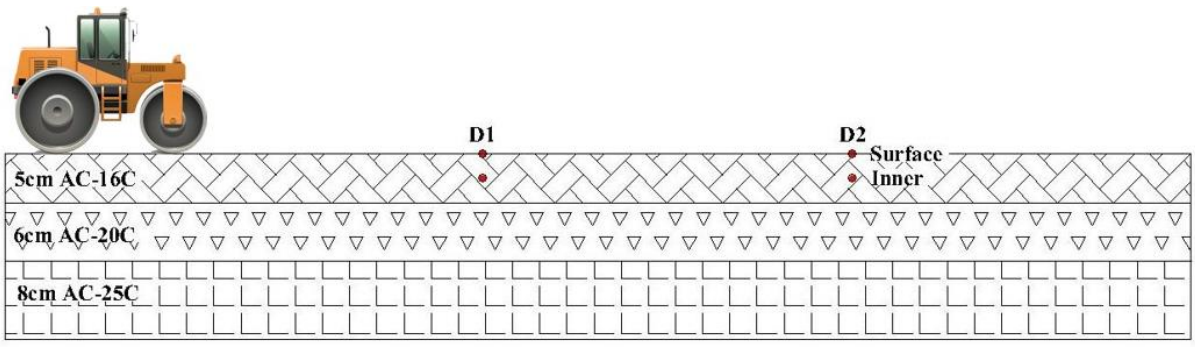


**Figure 4.** Compaction density monitoring roadway surface structure.

Two measurement points were randomly selected in the construction sections D1 and D2 when the density measurement was performed after each rolling by steel wheel or tire rollers. Test point density could be based on drill core sampling, measuring its gross bulk density to correct the density value further. At the same time, the HMA surface and internal temperatures were collected in real-time. The evolution properties of compaction density and the effect of migration and reorganization of aggregate particles were obtained under the synergistic influence of multi-physical fields from the compaction density measurements.

## 4. Results and discussions

This research statistically analyzed the temperature field, compaction thickness, and compaction density variation data during the HMA field compaction process of the AC-16 mid-surface layer and AC-16C upper layer, respectively. First, the evolution properties of temperature field, compaction thickness, and compaction density were established under the synergistic influence of multiple physical fields. Second, the synergistic relationship of multi-physical fields was analyzed from the compaction process of HMA. Finally, the effects of aggregate horizontal and vertical motions and aggregate particle migration and reorganization on the multi-physics fields were studied.

### *4.1. Temperature field test analysis*

The collected data was analyzed on the temperature field of the HMA compaction process, and the temperature variations were shown in Figures 5 and 6 at the two measurement points P1 and P2.

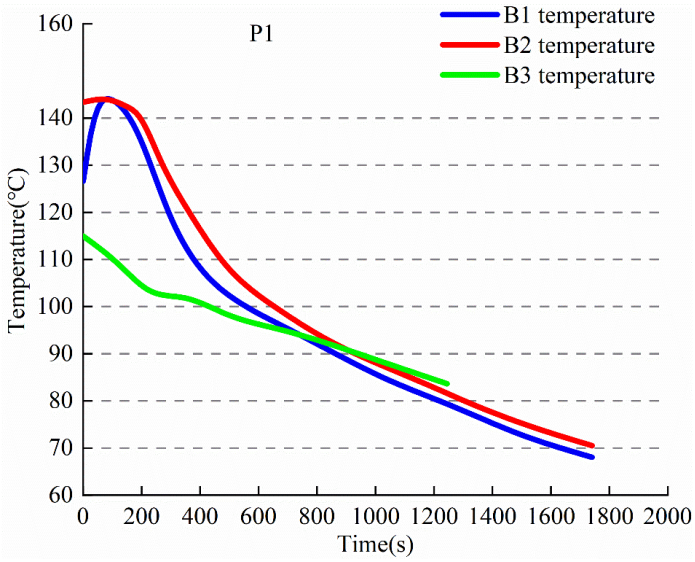


**Figure 5.** P1 Temperature versus time curve (B1, B2, and B3 represented the location of the middle and bottom of the layer surface, respectively).

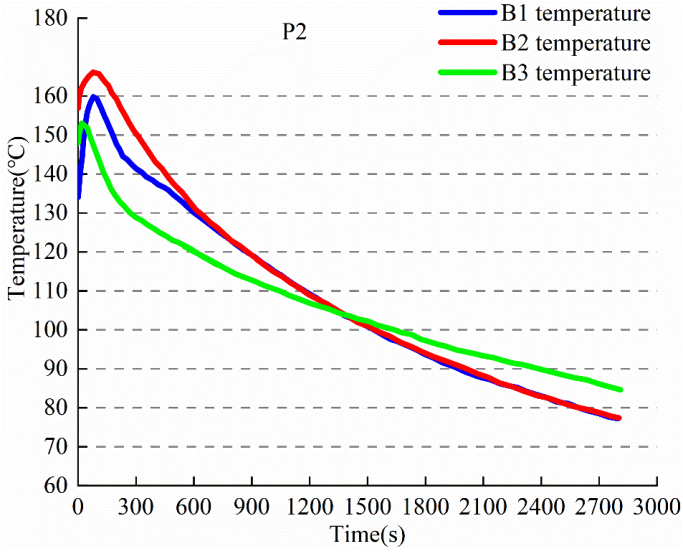


**Figure 6.** P2 Temperature versus time curve (B1, B2, and B3 represented the location of the middle and bottom of the layer surface, respectively).

HMA compaction process of the same measurement point of different layers of the temperature field showed that the measurement of the initial Pt100 sensors needed about 100 s to achieve synchronization with the temperature of the mixture (due to the layer bottom sensors in the paving buried in advance, measurement point P1 could not be shown with the temperature rise of the reflection time). When the initial temperature of the asphalt mixture $T_0$ was reduced to about 100 °C, the results showed that $T_{B2} > T_{B1} > T_{B3}$. Due to the temperature of the base of the mix being only about 20 °C, there is a need to absorb a large amount of heat to make the temperature rise to achieve the energy balance. At the same time, the mixed layer surface and the atmospheric environment (including solar

radiation, wind speed, convection, etc.), rolling tools' rapid heat transfer led to $T_{B1}$ lower than $T_{B2}$. Heat reduced the asphalt mixture temperature through the thermal conductivity of the layer surface and the bottom. When the asphalt mixture temperature dropped below 100 °C, the results showed that $T_{B3} > T_{B2} \approx T_{B1}$. Due to the bottom of the layer, the base of the temperature difference decreased, leading to a reduction in the rate of heat conduction. In contrast, the layer surface and the middle of the layer density increase led to the speed of heat conduction increase, and the layer surface and the outside world of the temperature difference still had more considerable heat convection and the heat radiation amount was strong.

The temperature fields of HMA showed that the temperatures of both measurement points P1 and P2 in the same layer tended to accelerate the cooling with the increase of the compaction density in the same layer at different measurement points during the compaction process. However, the rate of temperature drop of P1 and P2 was different. The initial temperature of P2 was higher than that of P1, but the decreasing rate of temperature of P1 was more extensive than that of P2. From Eqs (2) and (4), the heat transfer process of HMA was positively correlated with both density and initial temperature. The initial temperature played a vital role in the heat transfer rate of the compaction process of HMA from the monitoring data.

The temperature influencing factors of each layer were different during HMA field compaction, and there were differences in initial temperature during paving, which made the mixture's temperature drop at different rates. However, all layers conform to the properties of heat conduction, so the temperature change in the surface, the middle, and the bottom of the layer may have a cubic polynomial relationship with the rolling time. It was:

$$T_{HMA} = w_3 t^3 + w_2 t^2 + w_1 t + w_0 \tag{6}$$

where $T_{HMA}$ is the current temperature of the mixture (°C); $w_0$, $w_1$, $w_2$, and $w_3$ are the regression function coefficients related to the mixture's temperature and the compaction environment; and $t$ is the rolling time (s).

The regression statistical analysis of the temperature field of the HMA field compaction process could be, when taking the P2 measurement point as an example, obtained as the parameters $w_0$, $w_1$, $w_2$, and $w_3$ of temperature and time. The correlation coefficients $R^2$ were analyzed in correlation with the measurement points and the appropriate range values of each parameter were obtained, as shown in Table 1.

**Table 1.** P2 Temperature field variation for each parameter.

| P2 | $w_0$ | $w_1$ | $w_2$ | $w_3$ | $R^2$ | Regression equation |
|---|---|---|---|---|---|---|
| B1 | 152.33 | -0.03 | $-2.79*10^{-6}$ | $2.11*10^{-9}$ | 0.969 | $T = 2.11*10^{-9}t^3 - 2.79*10^{-6}t^2 - 0.03t + 152.33$ |
| B2 | 167.93 | -0.07 | $1.91*10^{-5}$ | $-2.17*10^{-9}$ | 0.993 | $T = -2.17*10^{-9}t^3 + 1.91*10^{-5}t^2 - 0.07t + 167.93$ |
| B3 | 148.83 | -0.06 | $2.85*10^{-5}$ | $-5.18*10^{-9}$ | 0.990 | $T = -5.18*10^{-9}t^3 + 2.85*10^{-5}t^2 - 0.06t + 148.83$ |

The test results showed that the compaction density of HMA increased rapidly with the number of rolling under the synergistic influence of multi-physical fields. The corresponding rates of heat conduction and convection accelerated accordingly, and the decreasing rate of the temperature field increased sharply. However, as the compaction density increased slowly or no longer increased, the rate of heat conduction no longer increased, and the corresponding rate of heat conduction, heat convection, and heat radiation of the HMA began to decrease as the temperature difference between the HMA and the surrounding decreased. Eventually, the decreasing rate of the temperature field tended to stabilize. Therefore, the cooling of the temperature field could be divided into two stages during the HMA compaction process, namely:

1) Accelerated cooling stage, in which the density $\rho$ of the mixture increased rapidly and $\Delta T$ grew rapidly with the increase of $\rho$.

2) Uniform cooling stage, in which the mix density $\rho$ increased slowly and $\Delta T$ stabilized with $\rho$ and no longer increased.

### *4.2. Compaction thickness test analysis*

The data measured by the level meter was analyzed, and the curve of variation of HMA thickness with the different rolling times was obtained under the synergistic influence of multiple physical fields, as shown in Figures 7 to 10.

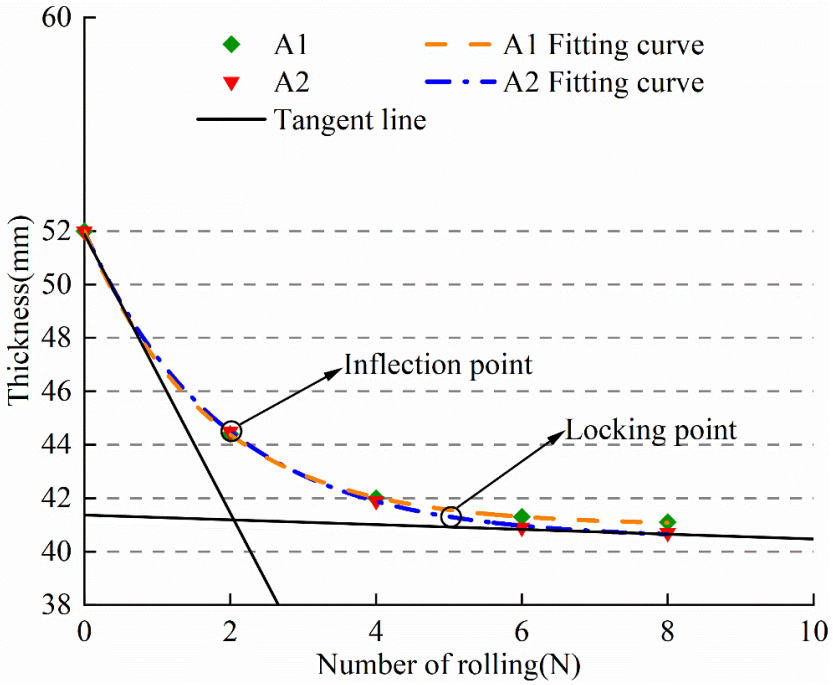


**Figure 7.** M1 Thickness variation curve.

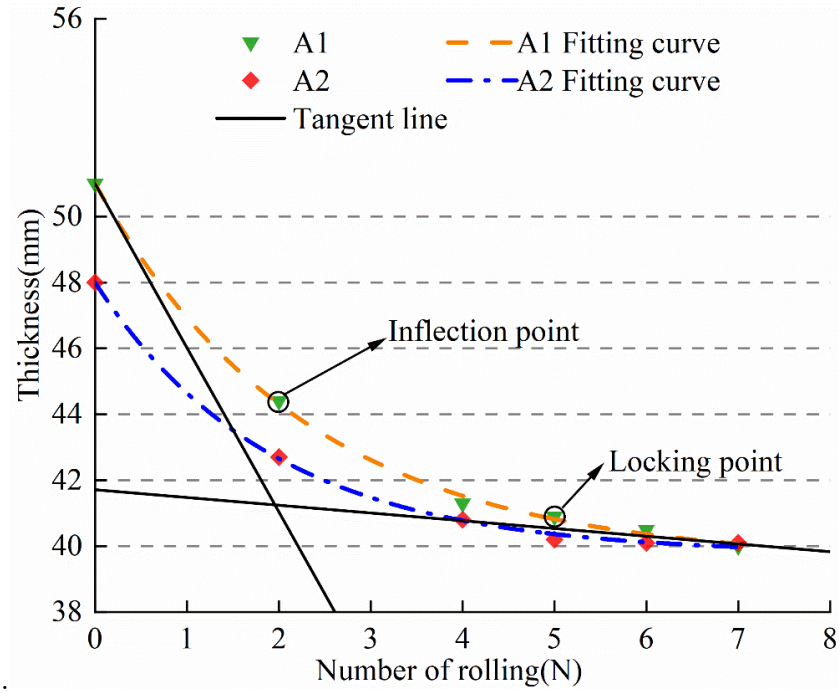


**Figure 8.** M2 Thickness variation curve.

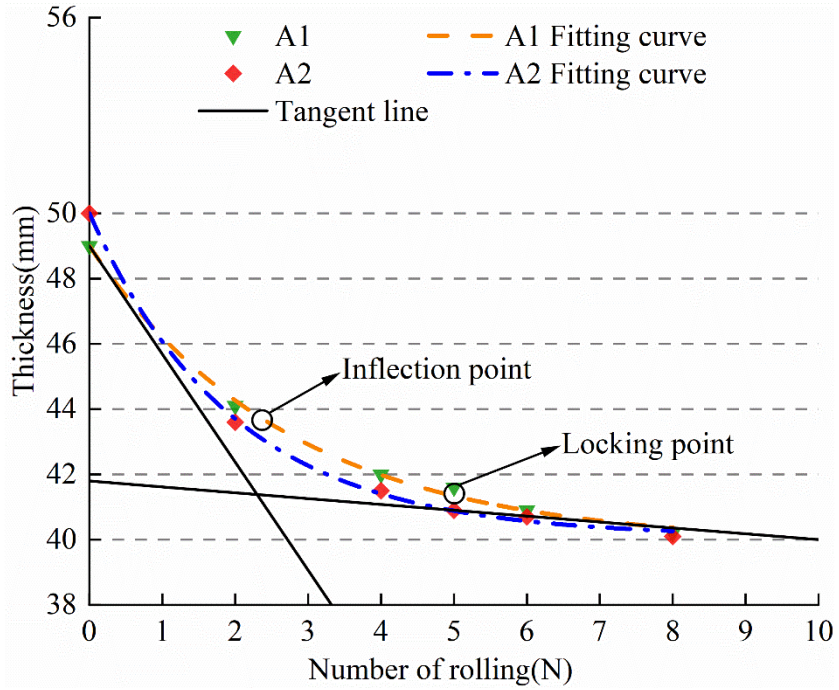


**Figure 9.** M3 Thickness variation curve.

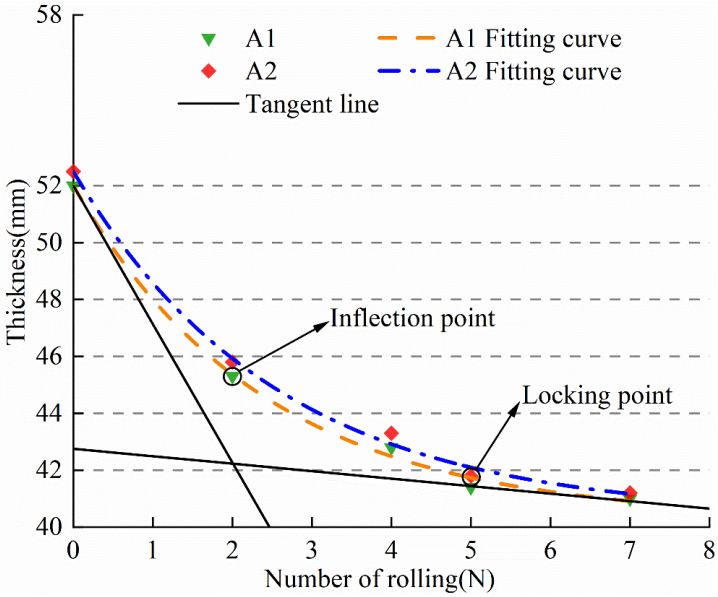


**Figure 10.** M4 Thickness variation curve.

The variation of thickness with the rolling times showed that the amount of thickness variation, $\Delta H$, was different due to the difference in the thickness of the loose pavement. When the initial rolling was done twice, $\Delta H$ ranged from 4 to 9 mm. When rolling 3~4 times, $\Delta H$ ranged from 1 to 3 mm. When rolling more than five times, $\Delta H$ was less than 1 mm with very little change. So, if only a single rolling method were used, the thickness of the compacted layer of asphalt mixture could be expressed by the following relationship [42]:

$$\frac{H_N - H_\infty}{H_\infty} = \frac{H_0 - H_\infty}{H_\infty} \times e^{-\alpha N} \tag{7}$$

where: $H_N$ is the layer thickness after rolling $N$ times, $H_\infty$ is the theoretical layer thickness after endless times of rolling, $H_0$ is the layer thickness at the beginning of rolling, $N$ is the number of times of rolling and $\alpha$ is the influencing factor of the deformation speed of rolling, which reflects the deformation capacity of the asphalt mixture in this state under a particular load and environmental effects. Transforming Eq (7) further, it could be obtained that:

$$H_N = H_\infty \times (1.0 + \gamma \times e^{-\alpha N}) \tag{8}$$

The parameter $\gamma = (H_0 - H_\infty)/H_\infty$ represents the correlation between the state before and the theoretical final compaction state.

Nonlinear regression analysis of the field measurement data could get the parameters $\alpha$, $\gamma$, and $H_\infty$ in the relationship between the thickness of the compacted layer and the rolling times passes. The correlation coefficient $R^2$ was analyzed in correlation with the measurement points and the appropriate range values of each parameter were obtained, as shown in Table 2.

**Table 2.** Variation of compaction thickness for each parameter.

| Test points | | $H_0$ | $H_\infty$ | $\gamma$ | $\alpha$ | $R^2$ | Regression equation |
|---|---|---|---|---|---|---|---|
| M1 | A1 | 52 | 41.0 | 0.27 | 0.59 | 0.99997 | $H_N = H_\infty * (1.0 + 0.27 * e^{-0.59*N})$ |
| | A2 | 52 | 40.5 | 0.28 | 0.53 | 0.99989 | $H_N = H_\infty * (1.0 + 0.28 * e^{-0.53*N})$ |
| M2 | A1 | 51 | 39.5 | 0.29 | 0.44 | 0.99875 | $H_N = H_\infty * (1.0 + 0.29 * e^{-0.44*N})$ |
| | A2 | 48 | 39.7 | 0.21 | 0.52 | 0.99882 | $H_N = H_\infty * (1.0 + 0.21 * e^{-0.52*N})$ |
| M3 | A1 | 49 | 40.1 | 0.22 | 0.37 | 0.99709 | $H_N = H_\infty * (1.0 + 0.22 * e^{-0.37*N})$ |
| | A2 | 50 | 40.0 | 0.25 | 0.50 | 0.99886 | $H_N = H_\infty * (1.0 + 0.25 * e^{-0.50*N})$ |
| M4 | A1 | 52 | 40.5 | 0.28 | 0.42 | 0.99638 | $H_N = H_\infty * (1.0 + 0.28 * e^{-0.42*N})$ |
| | A2 | 52.5 | 40.8 | 0.29 | 0.39 | 0.99603 | $H_N = H_\infty * (1.0 + 0.29 * e^{-0.39*N})$ |

The mean values $\gamma = 0.26$, $\alpha = 0.47$, and $R^2 = 0.99822$ were obtained by field test regression, then the functional expression of $H_N$ (mm) was obtained from Eq (8) as:

$$H_N = H_\infty * (1.0 + 0.26 * e^{-0.47*N}) \tag{9}$$

The above Eq (9) could be used to predict the compacted layer thickness. If $H_\infty \approx H_{design}$ was approximated, the compacted thickness of the asphalt mixture could be expressed as:

$$H_N = H_{design} * (1.0 + \gamma * e^{-\alpha*N}) \tag{10}$$

The cumulative value of thickness change of M3 was used as an example to analyze the change rule of structural layer thickness in the compaction process of HMA. Table 3 and Figure 11 showed that the "cumulative value of thickness change" has an excellent logarithmic correlation with the rolling times, i.e., $h = z\ Ln(N) + p$.

**Table 3.** Cumulative values of M3 degree change (mm) and regression equation.

| Number of rolling | A1 Thicknesses | Regression equation | A2 Thicknesses | Regression equation |
|---|---|---|---|---|
| 2 | 5.0 | *h = 2.74Ln(N) + 3.11* $R^2 = 0.995$ | 6.5 | *h= 2.48Ln(N) + 4.92* $R^2 = 0.979$ |
| 4 | 7.0 | | 8.5 | |
| 5 | 7.4 | | 9.1 | |
| 6 | 8.1 | | 9.3 | |
| 8 | 8.8 | | 9.9 | |

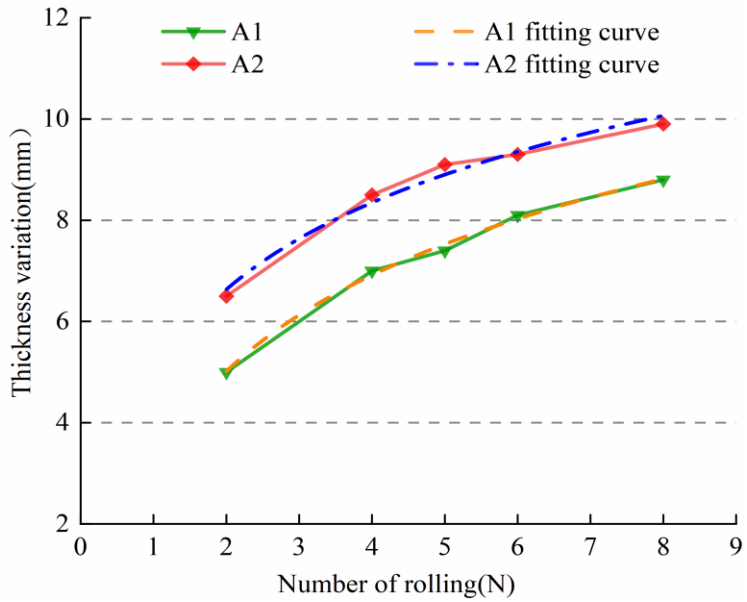


**Figure 11.** Cumulative change in M3 thickness versus number of rolling curves.

The inflection point [43] would appear near the rolling number 2, and thickness would be almost unchanged after the rolling number more than 5 times in the compaction process of the asphalt mixture from the tangent line intersection in Figures 7 to 10. Therefore, the point near the rolling number 5 could be defined as the locking point [44] of HMA field compaction. Thus, the field compaction process could be divided into three stages under the influence of multi-physical fields, namely:

1) Accelerated compaction stage, in which $\Delta H$ increased rapidly and $H_N$ quickly decreased with the increasing rolling numbers.

2) Uniform compaction stage, in which $\Delta H$ remained unchanged and $H_N$ decreased linearly with the increasing rolling numbers.

3) Decelerated compacting stage, in which $\Delta H$ decreased gradually and $H_N$ decreased slowly with the increasing rolling numbers.

The structural layer thickness decreased rapidly, the vertical and horizontal displacements of the aggregate particles increased considerably, and the vertical displacements were more significant than the horizontal displacements [45] during the accelerated compacting stage. It might be due to the increase in contacts and vertical unbalanced force of the aggregate particles. The thickness of the structural layer decreases uniformly, and the vertical and horizontal displacements of the aggregate particles begin to fall gradually in the uniform compaction stage. It could be due to the formation of skeleton structure among aggregates, the corresponding contact number of aggregates, and the vertical unbalance force beginning to decrease. The thickness of the structural layer decreased slowly or even unchanged, and the vertical and horizontal displacements of the aggregate particles almost ceased to increase and stabilized in the decelerated compacting stage. It could be attributed to the formation of the locking structure among the aggregate skeletons and the gradual formation of the densification structure.

The heat transfer rate was increased accordingly, with the thickness of HMA compaction decreased. The thinner the thickness, the faster the temperature field changes and the easier it was to be compacted as the number of rolling times increased for different thicknesses of points in the same temperature field. Therefore, the thickness of the compaction layer affected the change of the

temperature field, and the transformation of the temperature field involved the compaction difficulty of HMA. It was found that there was a synergistic influence between the change of compaction thickness and the change of temperature field from the change rule of compaction thickness.

### *4.3. Compaction thickness test analysis*

The variation of gross bulk density and temperature field of HMA with compaction time at different measurement points was shown in Figures 12 to 15.

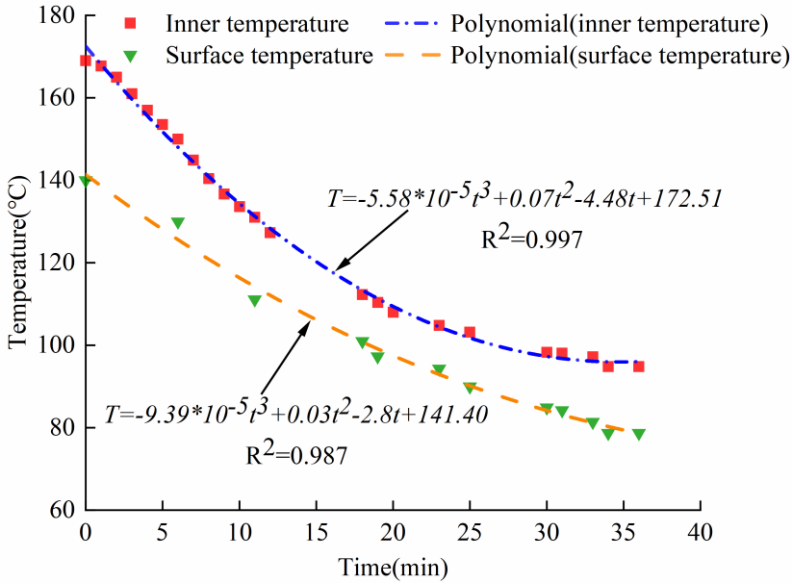


**Figure 12.** D1 Temperature over time.

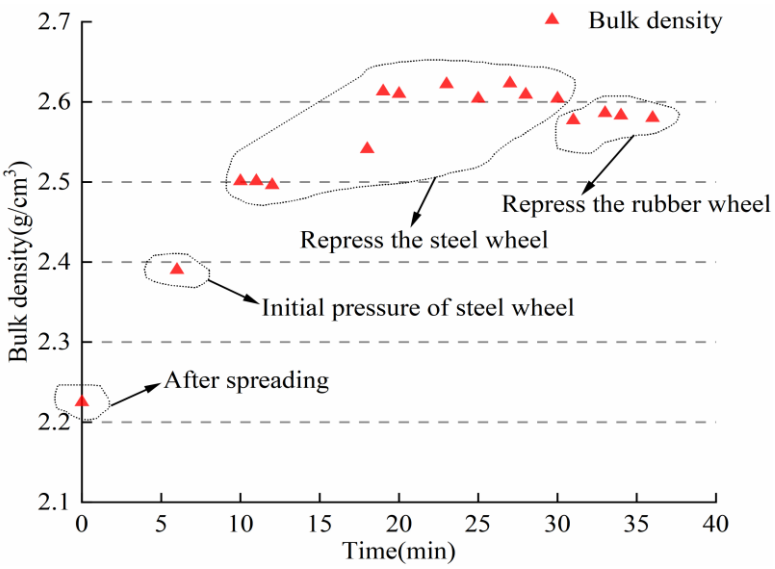


**Figure 13.** D1 Density over time.

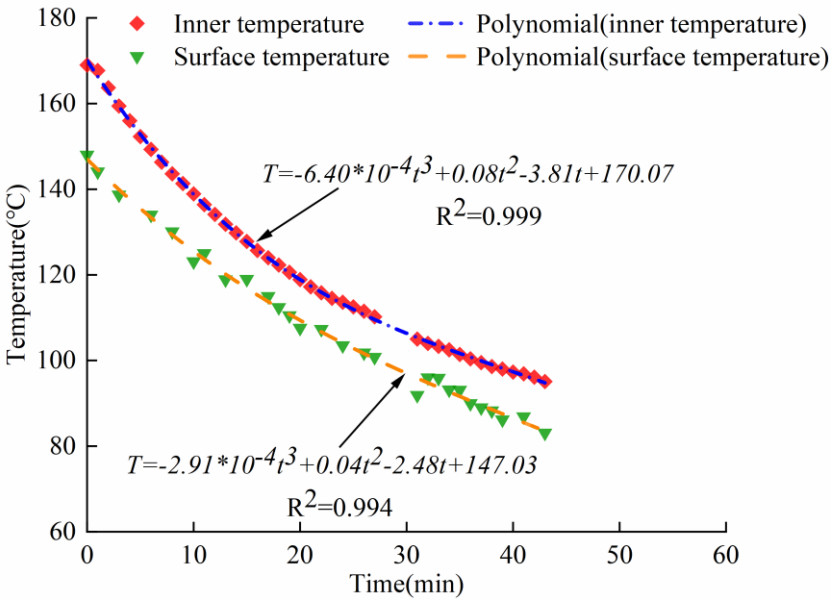


**Figure 14.** D2 Temperature over time.

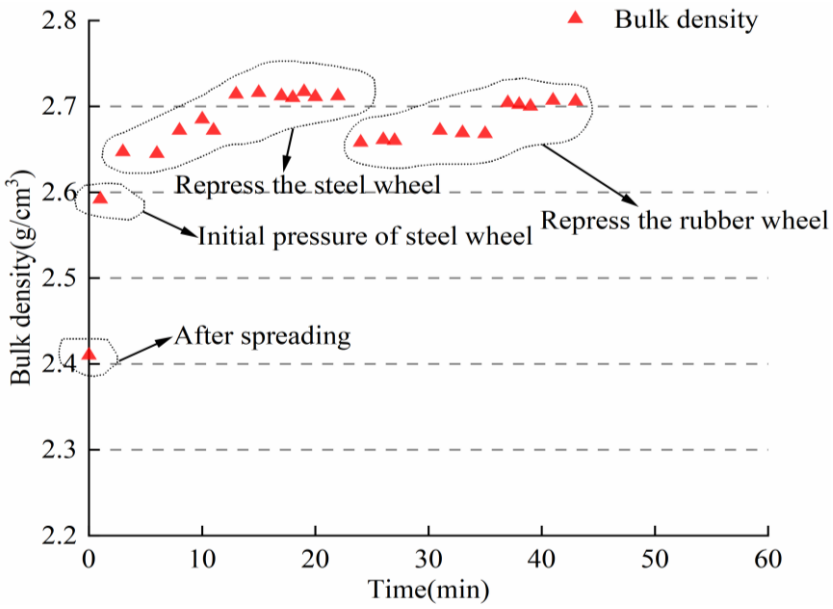


**Figure 15.** D2 Density over time.

Analysis from Figures 12 to 15 showed that the density of asphalt mixes underwent significant changes with the increase in the number of rolling (or time). The density of the mixture was low after loose paving, and the initial compression increased the density rapidly. The density increased further with the steel wheel vibration re-compacting, and the density was stabilized in the rolling three times after. The parallel test results showed that the density tends to change from large to small after the same rolling. It indicated the visco-plastic deformation and delayed recovery of visco-elastic deformation of the asphalt mixture. When kneading and re-compacting with rubber wheel rollers, the first two passes caused the insufficiently compacted mixture to be subjected to significant shear

stresses and to push and arch. It resulted in a tendency for the mix densities to decrease but gradually increased again after several rollings. The rubber roller on the mix rubbing and kneading action reduced aggregate damage, eliminated stress cracks, and improved the surface "oiliness". The purpose of static steel wheel final compaction was to stop the wheel tracks left by the rolling process of the tire roller, and it did not improve the compactness. It should be carried out immediately after the end of the re-compaction. Otherwise, it could be challenging to eliminate the wheel tracks after the temperature was too low.

The type of roller affected the temperature field of the HMA. Steel wheel rollers caused a significant temperature drop in the surface of the HMA. In contrast, rubber wheel rollers had little effect on the surface temperature of the HMA and even had an instantaneous increase. The temperature difference between the middle and surface of the HMA layer was about 10 to 20 °C under the combination of steel and rubber wheel rolling. In the AC-16C compaction process, the surface and middle layer temperatures had the same three-degree polynomial relationship with the rolling times. The regression statistical analysis of the temperature fields of the two measurement points, D1 and D2, respectively, were shown in Tables 4 and 5:

**Table 4.** D1 Temperature field variation for each parameter.

| D1 | $W_0$ | $W_1$ | $W_2$ | $W_3$ | $R^2$ | Regression equation |
|---|---|---|---|---|---|---|
| Surface | 141.40 | -2.83 | 0.03 | $-9.39*10^{-5}$ | 0.9875 | $T = -9.39*10^{-5}t^3 + 0.03t^2 - 2.83t + 141.40$ |
| Inner | 172.51 | -4.48 | 0.07 | $-5.58*10^{-5}$ | 0.9969 | $T = -5.58*10^{-5}t^3 + 0.07t^2 - 4.48t + 172.51$ |

**Table 5.** D2 Temperature field variation for each parameter.

| D2 | $W_0$ | $W_1$ | $W_2$ | $W_3$ | $R^2$ | Regression equation |
|---|---|---|---|---|---|---|
| Surface | 147.03 | -2.48 | 0.04 | $-2.91*10^{-4}$ | 0.9939 | $T = -2.91*10^{-4}t^3 + 0.04t^2 - 2.48t + 147.03$ |
| Inner | 170.06 | -3.81 | 0.08 | $-6.40*10^{-4}$ | 0.9996 | $T = -6.40*10^{-4}t^3 + 0.08t^2 - 3.81t + 170.06$ |

The accuracy of the regression statistical analysis of the temperature field of HMA was thus verified again under the influence of multiple physical fields. The monitoring results of the compaction density showed that, to ensure adequate compaction of the modified asphalt mixture, the effective rolling time was around 25 min. At the end of the rolling, the internal temperature was not less than 100 °C (the surface temperature was not less than 90 °C).

The variation of gross bulk density with compaction temperature at the surface and middle of the HMA layer at the two measurement points, D1 and D2, was shown in Figures 16 to 19.

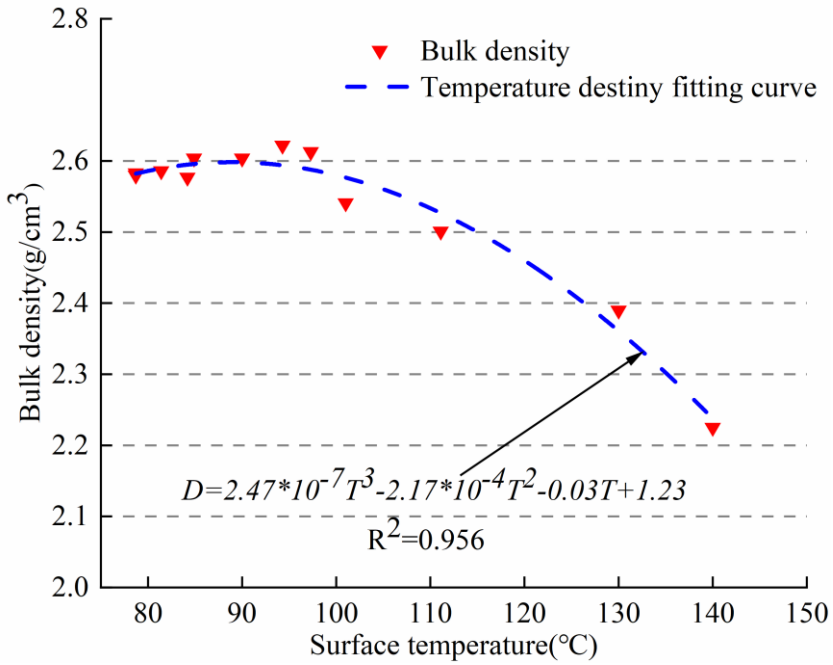


**Figure 16.** Variation of D1 density with layer surface temperature.

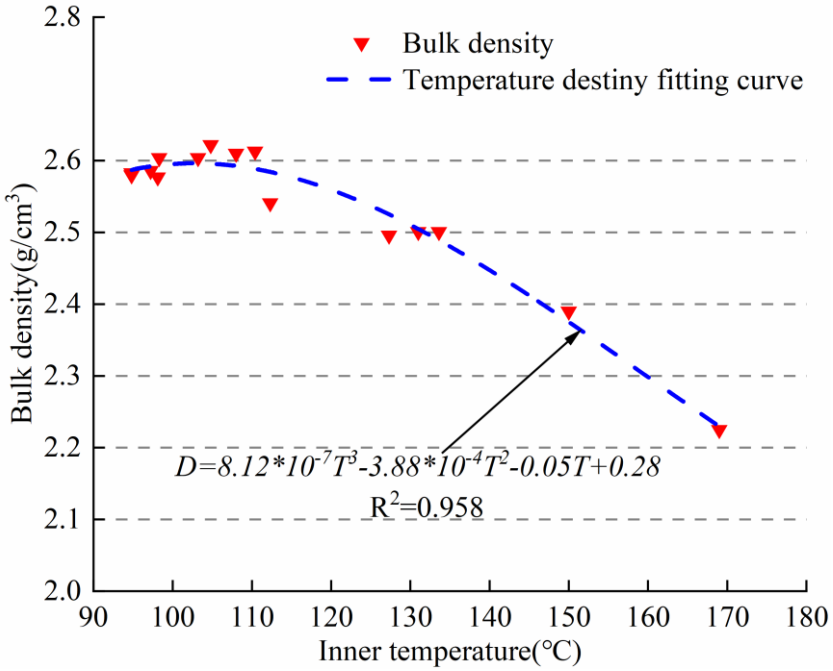


**Figure 17.** Variation of D1 density with temperature in the layer.

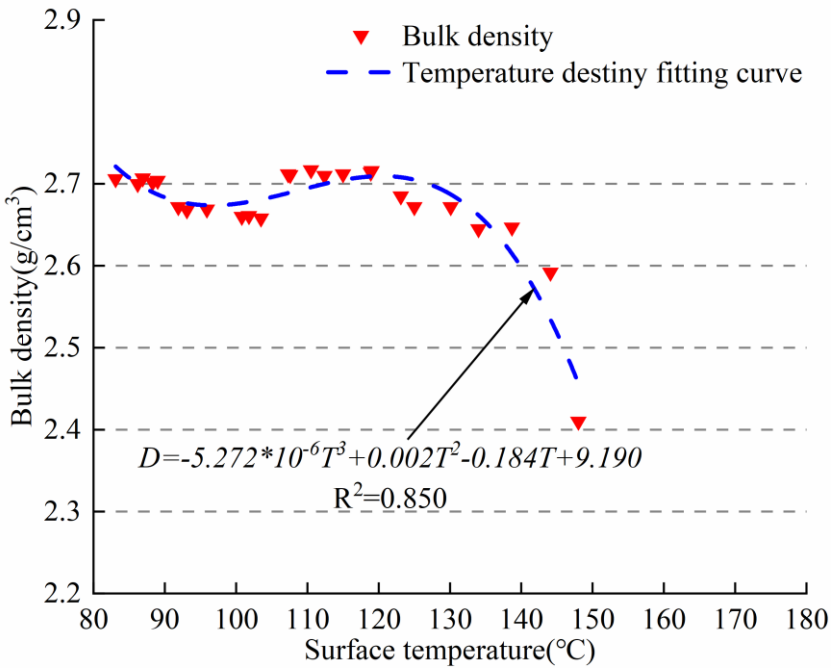


**Figure 18.** Variation of D2 density with layer surface temperature.

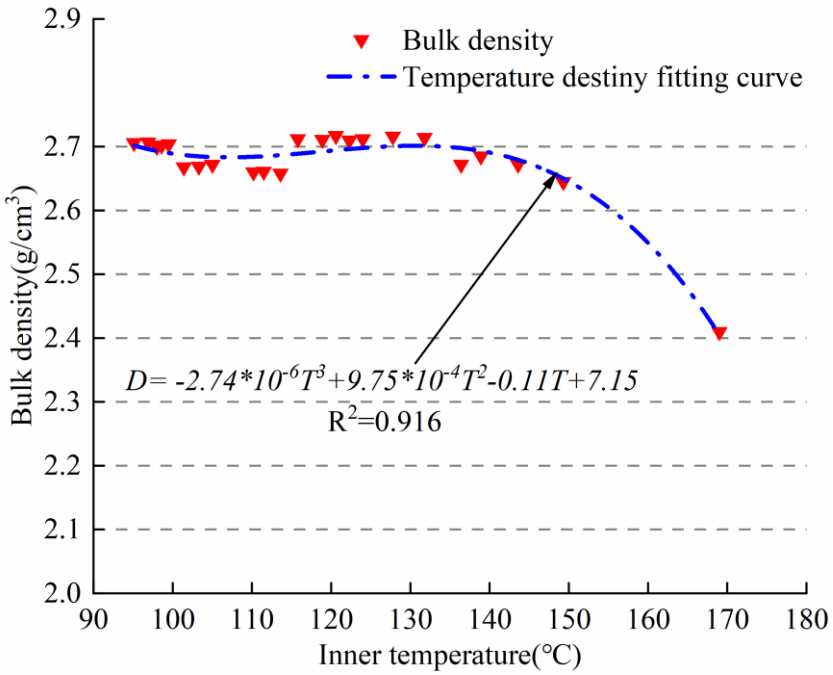


**Figure 19.** Variation of D2 density with temperature in the layer.

The results showed differences in the temperature fields at the surface and middle of the layer during the compaction process of HMA, and they led to different rates of change in the compaction density. However, the compaction density had the same variation rule as the temperature field under the synergistic influence of multi-physical fields. The research found that there might be a three-degree

polynomial relationship between density change and temperature during compaction, which was:

$$D_{HMA} = p_3T^3 + p_2T^2 + p_1T + p_0 \tag{11}$$

where $D_{HMA}$ is the density of HMA (g/cm$^3$); $p_0$, $p_1$, $p_2$, $p_3$ are the coefficients of the regression function related to the temperature of the mixture and the compaction environment as well as the compaction process; and $T$ is the temperature of the rolling process (°C).

Regression statistical analysis of the density was performed to obtain the parameters $p_0$, $p_1$, $p_2$, and $p_3$ in Eq (11) under the synergistic influence of the multi-physical fields at the two measurement points D1 and D2. The correlation coefficients, $R^2$, were then correlated with the measurement points, and the appropriate range of values of each parameter was obtained, as shown in Tables 6 and 7.

**Table 6.** Variation of D1 compaction density for each parameter.

| D1 | $p_0$ | $p_1$ | $p_2$ | $p_3$ | $R^2$ | Regression equation |
|---|---|---|---|---|---|---|
| Surface | 1.23 | -0.03 | $-2.17*10^{-4}$ | $2.47*10^{-7}$ | 0.956 | $D = 2.47*10^{-7}T^3 - 2.17*10^{-4}T^2 - 0.03T + 1.23$ |
| Inner | 0.28 | -0.05 | $-3.88*10^{-4}$ | $8.12*10^{-7}$ | 0.958 | $D = 8.12*10^{-7}T^3 - 3.88*10^{-4}T^2 - 0.05T + 0.28$ |

**Table 7.** Variation of D2 compaction density for each parameter.

| D2 | $p_0$ | $p_1$ | $p_2$ | $p_3$ | $R^2$ | Regression equation |
|---|---|---|---|---|---|---|
| Surface | 9.190 | -0.184 | 0.002 | $-5.272*10^{-6}$ | 0.850 | $D = -5.272*10^{-6}T^3 + 0.002T^2 - 0.184T + 9.190$ |
| Inner | 7.15 | -0.11 | $9.75*10^{-4}$ | $-2.74*10^{-6}$ | 0.916 | $D = -2.74*10^{-6}T^3 + 9.75*10^{-4}T^2 - 0.11T + 7.15$ |

The spatial distribution of pores was influenced by the compaction method [46] in the HMA during compaction. The void ratio gradually decreases, and the density increases continuously in the static load method compaction process with the number of rolls. At the same time, the aggregate was constrained to increase, and the aggregate was crushed severely so that the density reached a bottleneck and could not continue to grow. However, the dynamic load action of the rubber roller caused the crushed aggregate to migrate, which tended to reduce the density of the HMA. The kneading action of the rubber rollers will effectively reorganize the broken aggregate to protect the aggregate from further crushing. Eventually, the mixture skeleton reorganization reduced the void ratio again to form a new stable skeleton structure. The additional increased density of HMA will directly affect the change in the temperature field. Therefore, the migration and reorganization of aggregate particles impacted the evolution process of the multi-physics field under different compaction methods. When the rolling temperature was lower than 85°C, the density of the HMA was almost unchanged with the increase in the number of rolls and the void ratio no longer decreased and stabilized. Therefore, the movement of aggregate particles significantly reduced with the stabilization of the compaction thickness, the

decrease of temperature, and the increasing viscosity of asphalt.

The temperature of the layer surface was significantly lower than that of the layer center during HMA field compaction due to the more vigorous thermal convection and heat conduction at the layer surface relative to the layer center. What's more, the density change of the layer surface was faster than that of the middle layer, which led to a further acceleration of the heat dissipation rate of the layer surface—and ultimately led to a more drastic change of the temperature field of the layer surface than that of the middle layer. The evolution of the temperature field influenced the size of the void ratio, which in turn affected the change in compaction density. There was a synergistic influence among the multiple physical fields in the compaction process of HMA.

In summary, this study could provide intelligent compaction with the principle of multi-physical field synergy of on-site compaction and the method of analyzing and processing each parameter. The compaction process could be effectively predicted by the relationship between temperature field and time, compaction thickness and number of times, and compaction density and temperature. First, the prediction could improve the efficiency of construction organizations. Second, controlling the number of times and time of rolling to avoid the under-compaction and over-compaction problems of HMA could help to improve the efficiency of construction machinery. Finally, this method could improve the construction quality of HMA through exemplary construction process management.

## 5. Conclusions

This research evaluated the influence of the temperature field, compaction thickness, and compaction density during HMA field compaction. It was finally concluded that there was a synergistic effect among the multiple physical fields of the HMA during the compaction process. The conclusions of this research were as follows:

1) A two-stage change during HMA field compaction characterized the synergistic influence of compaction density and temperature field. There were cubic polynomial evolution properties between the temperature field and time under the synergistic impact of multiple physical fields.

2) The compaction process could be characterized by three different stages changing under the synergistic influence of compaction thickness and temperature field. There was an exponential relationship between the thickness of the compacted layer and the number of rolls under the synergistic influence of multiple physical fields.

3) The displacements of aggregate particles showed movement directions that were faster and then slower, and the vertical displacement was more significant than the horizontal displacement in the three phases of compaction under the synergistic influence of multiple physical fields.

4) The aggregate particles showed a direction of vertical to horizontal migration and reorganization with the compaction process from static to dynamic loads under the synergistic influence of the multi-physics fields. The migration and reorganization of aggregate particles also affected the evolution of the multi-physics fields.

5) This study revealed the synergistic properties of multi-physical fields in the compaction process of HMA. The construction compaction theory could be further improved by more physical engineering applications and verified by data monitoring.

## Use of AI tools declaration

The authors declare they have not used Artificial Intelligence (AI) tools in the creation of this article.

## Acknowledgments

The research was supported by Major Projects of Xiangjiang Laboratory (grant number: 22XJ01009); the National Natural Science Foundation of China (grant number: 52178414; 52078065, 52227815); and the Science and Technology Innovation Program of Hunan Province (grant number: 2020RC4048).

## Conflict of interest

The authors declare there is no conflict of interest.

## References

1. R. N. Linden, J. P. Mahoney, N. C. Jackson, Effect of compaction on asphalt concrete performance, *Transp. Res. Rec.*, **1217** (1989), 20–28. https://onlinepubs.trb.org/Onlinepubs/trr/1989/1217/1217-003.pdf
2. X. Zhao, D. Niu, P. Zhang, Y. Niu, H. Xia, P. Liu, Macro-meso multiscale analysis of asphalt concrete in different laboratory compaction methods and field compaction, *Constr. Build. Mater.*, **361** (2022), 129607. https://doi.org/10.1016/j.conbuildmat.2022.129607
3. H. Zhang, H. Ding, A. Rahman, Effect of asphalt mortar viscoelasticity on microstructural fracture behavior of asphalt mixture based on cohesive zone model, *J. Mater. Civ. Eng.*, **34** (2022), 04022122. https://doi.org/10.1061/(ASCE)MT.1943-5533.0004277
4. H. Wang, C. Wang, Z. You, X. Yang, Z. Huang, Characterising the asphalt concrete fracture performance from X-ray CT Imaging and finite element modelling, *Int. J. Pavement Eng.*, **19** (2018), 307–318. https://doi.org/10.1080/10298436.2017.1347440
5. P. Liu, H. Xu, D. Wang, C. Wang, C. Schulze, M. Oeser, Comparison of mechanical responses of asphalt mixtures manufactured by different compaction methods, *Constr Build Mater.*, **162** (2018), 765–780. https://doi.org/10.1016/j.conbuildmat.2017.12.082
6. W. Liu, Y. Gao, X. Huang, L. Li, Investigation of motion of coarse aggregates in asphalt mixture based on virtual simulation of compaction test, *Int. J. Pavement Eng.*, **21** (2018), 1–13. https://10.1080/10298436.2018.1447109
7. W. Liu, X. Gong, Y. Gao, L. Li, Evaluation, Microscopic characteristics of field Compaction of asphalt mixture using discrete element method, *J. Test. Eval.*, **47** (2019), 20180633. https://10.1520/JTE20180633
8. X. Yang, Z. You, C. Jin, H. Wang, Aggregate representation for mesostructure of stone based materials using a sphere growth model based on realistic aggregate shapes, *Mater. Struct.*, **49** (2016), 2493–2508. https://10.1617/s11527-015-0662-y
9. Q. Liu, J. Hu, P. Liu, J. Wu, M. Oeser, Uncertainty analysis of in-situ pavement compaction considering microstructural characteristics of asphalt mixtures, *Constr. Build. Mater.*, **279** (2021), 122514. https://10.1016/j.conbuildmat.2021.122514

10. C. Zhang, H. Yu, X. Zhu, D. Yao, X. Peng, X. Fan, Unified characterization of rubber asphalt mixture strength under different stress loading paths, *J. Mater. Civ. Eng.*, **36** (2024), 04023498. https://doi.org/10.1061/JMCEE7.MTENG-16145
11. T. Huang, Z. Wang, H. Dong, H. Qin, H. Liu, Z. Cao, Time-temperature-stress equivalent characteristics and nonlinear viscoelastic model of asphalt mixture under triaxial compressive stress state, *J. Mater. Civ. Eng.*, **36** (2024), 04023543. https://doi.org/10.1061/JMCEE7.MTENG-16679
12. H.Y. Ahmed, Methodology for determining most suitable compaction temperatures for hot mix asphalt, *J. Eng. Sci.*, (2007), 1235–1253. https://10.21608/jesaun.2007.114551
13. D. Jin, K. A. Boateng, S. Chen, K. Xin, Z. You, Comparison of rubber asphalt with polymer asphalt under long-term aging conditions in Michigan, *Sustainability*, **14** (2022). https://doi.org/10.3390/su141710987
14. Y. Gao, X. Huang, W. Yu, The compaction characteristics of hot mixed asphalt mixtures, *J. Wuhan Univ. Technol.-Mater. Sci. Ed.*, **29** (2014), 956–959. https://10.1007/s11595-014-1027-z
15. P. Liu, C. Wang, W. Lu, M. Moharekpour, M. Oeser, D. Wang, Development of an FEM-DEM model to investigate preliminary compaction of asphalt pavements, *Buildings*, **12** (2022), 932. https://doi.org/10.3390/buildings12070932
16. S. Komaragiri, A. Gigliotti, A. Bhasin, Feasibility of using a physics engine to virtually compact asphalt mixtures in a gyratory compactor, *Constr. Build. Mater.*, **308** (2021), 124977. https://doi.org/10.1016/j.conbuildmat.2021.124977
17. S. Komaragiri, A. Gigliotti, A. Bhasin, Calibration and extended validation of a virtual asphalt mixture compaction model using bullet physics engine, *Constr. Build. Mater.*, **311** (2021), 125257. https://doi.org/10.1016/j.conbuildmat.2021.125257
18. X. Wang, S. Shen, H. Huang, Meso-scale kinematic responses of asphalt mixture in both field and laboratory compaction, *Transp. Res. Rec.*, **2675** (2021), 1631–1642. https://doi.org/10.1177/03611981211009222
19. X. Wang, H. Huang, E. Tutumluer, J. S. Tingle, S. Shen, Monitoring particle movement under compaction using smartrock sensor: a case study of granular base layer compaction, *Transp. Geotech.*, **34** (2022), 100764. https://doi.org/10.1016/j.trgeo.2022.100764
20. D. Zhang, Z. Cheng, D. Geng, S. Xie, T. Wang, Experimental and numerical analysis on mesoscale mechanical behavior of coarse aggregates in the asphalt mixture during gyratory compaction, *Processes*, **10** (2021), 47. https://doi.org/10.3390/pr10010047
21. Z. Liu, L. Sun, J. Li, L. Liu, Effect of key design parameters on high temperature performance of asphalt mixtures, *Constr. Build. Mater.*, **348** (2022), 128651. https://doi.org/10.1016/j.conbuildmat.2022.128651
22. H. C. Dan, D. Yang, L. H. Zhao, S. P. Wang, Z. Zhang, Meso-scale study on compaction characteristics of asphalt mixtures in Superpave gyratory compaction using SmartRock sensors, *Constr. Build. Mater.*, **262 (**2020), 120874. https://doi.org/10.1016/j.conbuildmat.2020.120874
23. C. Shi, G. Qian, C. Hu, H. Yu, X. Gong, C. Zhang, et al., Experimental study of aggregate skeleton shear properties for asphalt mixture under different compaction stages, *Constr. Build. Mater.*, **404** (2023), 133123. https://doi.org/10.1016/j.conbuildmat.2023.133123
24. H. C. Dan, D. Yang, X. Liu, A. P. Peng, Z. Zhang, Experimental investigation on dynamic response of asphalt pavement using SmartRock sensor under vibrating compaction loading, *Constr. Build. Mater.*, **247** (2020) 118592. https://10.1016/j.conbuildmat.2020.118592

25. D. Jin, L. Yin, L. Malburg, Z. You, Laboratory evaluation and field demonstration of cold in-place recycling asphalt mixture in Michigan low-volume road, *Case Stud. Constr. Mater.*, **20** (2024), e02923. https://doi.org/10.1016/j.cscm.2024.e02923
26. A. Sha, X. Ren, J. Li, W. Jiang, M. Jia, Densification behavior of asphalt mixture and its relation with particle dynamic responses during gyratory compaction, *Constr. Build. Mater.*, **377** (2023), 131138. https://doi.org/10.1016/j.conbuildmat.2023.131138
27. X. Wang, S. Shen, H. Huang, Z. Zhang, Towards smart compaction: Particle movement characteristics from laboratory to the field, *Constr. Build. Mater.*, **218** (2019), 323–332. https://10.1016/j.conbuildmat.2019.05.122
28. Z. Cheng, D. Zhang, S. Xie, P. A. Polaczyk, T. Wang, SmartRock-based research on gyratory locking point for stone mastic asphalt mixture, *Buildings*, **12** (2022), 97. https://doi.org/10.3390/buildings12020097
29. X. Zhao, D. Niu, Y. Niu, B. Hu, X. Chen, P. Liu, Effect of compaction parameter on aggregate particle migration and compaction mechanism using 2D image analysis, *Constr. Build. Mater.*, **382** (2023), 131298. https://doi.org/10.1016/j.conbuildmat.2023.131298
30. X. Cai, K. Wu, W. Huang, Study on the optimal compaction effort of asphalt mixture based on the distribution of contact points of coarse aggregates, *Road Mater. Pavement Des.*, **22** (2021), 1594–1615. https://doi.org/10.1080/14680629.2019.1710238
31. D. Jin, D. Ge, J. Wang, L. Malburg, Z. You, Reconstruction of asphalt pavements with crumb rubber modified asphalt mixture in cold region: Material characterization, construction, and performance, *Materials*, **16** (2023). https://doi.org/10.3390/ma16051874
32. H. Yu, C. Zhang, G. Qian, J. Ge, X. Zhu, D. Yao, et al., Characterization and evaluation of coarse aggregate wearing morphology on mechanical properties of asphalt mixture, *Constr. Build. Mater.*, **388** (2023), 131299. https://doi.org/10.1016/j.conbuildmat.2023.131299
33. D. Jin, T. K. Meyer, S. Chen, K. A. Boateng, J. M. Pearce, Z. You, Evaluation of lab performance of stamp sand and acrylonitrile styrene acrylate waste composites without asphalt as road surface materials, *Constr. Build. Mater.*, **338** (2022), 127569. https://doi.org/10.1016/j.conbuildmat.2022.127569
34. C. Y. Ribas, L. P. Thives, Evaluation of effect of compaction method on the macrostructure of asphalt mixtures through digital image processing under Brazilian conditions, *Constr. Build. Mater.*, **228** (2019), 116821. https://doi.org/10.1016/j.conbuildmat.2019.116821
35. C. Wang, M. Moharekpour, Q. Liu, Z. Zhang, P. Liu, M. Oeser, Investigation on asphalt-screed interaction during pre-compaction: Improving paving effect via numerical simulation, *Constr. Build. Mater.*, **289** (2021), 123164. https://doi.org/10.1016/j.conbuildmat.2021.123164
36. Y. Li, Y. Yao, X. Shi, L. Zhang, G. Li, S. Pei, Study on vacuum compaction of asphalt mixture and its compaction performance, in *IOP Conference Series: Earth and Environmental Science*, **455** (2020), 012091. https://10.1088/1755-1315/455/1/012091
37. M. Hu, W. Jia, Z. Liu, J. Zhang, Y. Yao, Z. Shen, Experimental study on the characteristics of air voids of asphalt mixture under vacuum compaction, in *IOP Conference Series: Earth and Environmental Science*, **719** (2021), 032069. https://10.1088/1755-1315/719/3/032069
38. D. Jin, K. A. Boateng, D. Ge, T. Che, L. Yin, W. Harrall, et al., A case study of the comparison between rubberized and polymer modified asphalt on heavy traffic pavement in wet and freeze environment, *Case Stud. Constr. Mater.*, **18** (2023), e01847. https://doi.org/10.1016/j.cscm.2023.e01847

39. G. Qian, Z. He, H. Yu, X. Gong, J. Sun, Research on the affecting factors and characteristic of asphalt mixture temperature field during compaction, *Constr. Build. Mater.*, **257** (2020), 119509. https://doi.org/10.1016/j.conbuildmat.2020.119509
40. L. Chu, B. Zhu, T. Fwa, Prediction of temperature cooling trend of asphalt mixtures, in *IOP Conference Series: Materials Science and Engineering*, (2021), 012030. https://doi.org/10.1088/1757-899X/1075/1/012030
41. S. Maruyama, S. Moriya, Newton's Law of Cooling: Follow up and exploration, *Int. J. Heat Mass Transf.*, **164** (2021), 120544. https://doi.org/10.1016/j.ijheatmasstransfer.2020.120544
42. H. Lodewikus, *Compaction of Asphalt Road Pavements: Using Finite Elements and Critical State Theory*, Ph.D thesis, University of Twente, Enschede, 2004.
43. X. Qiu, J. Xu, W. Xu, S. Xiao, F. Wang, J. Yuan, Characterization of fatigue damage mechanism of asphalt mixtures with acoustic emission, *Constr. Build. Mater.*, **240** (2020), 117961. https://doi.org/10.1016/j.conbuildmat.2019.117961
44. Z. Cheng, X. Jia, H. Jiang, W. Hu, B. Huang, Quantification of impact compaction locking point for asphalt mixture, *Constr. Build. Mater.*, **302** (2021), 124410. https://doi.org/10.1016/j.conbuildmat.2021.124410
45. X. Zhu, G. Qian, H. Yu, D. Yao, C. Shi, C. Zhang, Evaluation of coarse aggregate movement and contact unbalanced force during asphalt mixture compaction process based on discrete element method, *Constr. Build. Mater.*, **328** (2022), 127004. https://doi.org/10.1016/j.conbuildmat.2022.127004
46. Y. Li, W. Jiang, J. Shan, P. Li, R. Lu, B. Lou, Characteristics of void distribution and aggregate degradation of asphalt mixture specimens compacted using field and laboratory methods, *Constr. Build. Mater.*, **270** (2021), 121488. https://doi.org/10.1016/j.conbuildmat.2020.121488



AIMS Press